Geochemistry 83 (2023) 126007

Contents lists available at ScienceDirect

Geochemistry

journal homepage: www.elsevier.com/locate/chemer

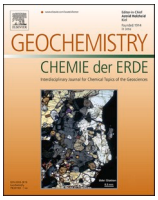

Spurious molybdenum isotope anomalies resulting from non-exponential mass fractionation

Gerrit Budde [a,b,c,*], François L.H. Tissot [c], Thorsten Kleine [b,d], Ren T. Marquez [c]

[a] Department of Earth, Environmental and Planetary Sciences, Brown University, Providence, RI 02912, USA
[b] Institut für Planetologie, University of Münster, 48149 Münster, Germany
[c] The Isotoparium, Division of Geological and Planetary Sciences, California Institute of Technology, Pasadena, CA 91125, USA
[d] Max Planck Institute for Solar System Research, 37077 Göttingen, Germany

ARTICLE INFO

Handling Editor: Mason Neuman

Keywords:
Mo isotopes
Mass-dependent fractionation
Bulk silicate Earth
Mantle heterogeneities
Nucleosynthetic anomalies
Exponential law

ABSTRACT

Mass-independent (nucleosynthetic) Mo isotope anomalies are uniquely useful for constraining genetic relationships among meteoritic and planetary materials and, by extension, the origin and nature of Earth's late-stage building blocks. The meaningful interpretation of such data, however, critically depends on the accurate correction of any natural and analytical mass-dependent isotope fractionation, which is commonly assumed to follow the 'exponential law'. Here, using new high-precision Mo isotope data for a diverse set of terrestrial samples, we show that mass-dependent Mo isotope fractionation in nature typically does not adhere to this law, but is instead dominated by equilibrium and Rayleigh processes. We demonstrate that even moderate degrees of such non-exponential fractionation (*i.e.*, mass-dependent isotope fractionation deviating from the exponential law) can result in significant spurious mass-independent Mo isotope anomalies that, when misinterpreted as nucleosynthetic anomalies, can lead to erroneous conclusions, particularly with respect to Earth's accretion history. Consequently, assessing the magnitude and origin of mass-dependent fractionation will be essential for future efforts to precisely determine the mass-independent Mo isotope composition of bulk silicate Earth and to identify potential nucleosynthetic isotope anomalies in terrestrial rocks.

1. Introduction

Nucleosynthetic isotope anomalies are mass-independent isotope variations resulting from the heterogeneous distribution of presolar matter, which makes them a formidable cosmochemical tool for constraining genetic relationships between meteoritic and planetary materials (*e.g.*, Dauphas and Schauble, 2016). An element that has proven uniquely powerful in this regard is molybdenum (Mo), because (*i*) it is relatively abundant in almost all types of Solar System materials, (*ii*) there are large nucleosynthetic isotope variations among bulk meteorites, and (*iii*) it can clearly distinguish between different nucleosynthetic processes (*e.g.*, Burkhardt et al., 2011; Budde et al., 2019). Most significantly, Mo isotope systematics have revealed a fundamental difference between 'non-carbonaceous' (*i.e.*, ordinary/enstatite chondrite-related) and 'carbonaceous' (*i.e.*, carbonaceous chondrite-related) meteorites (Budde et al., 2016), and that this so-called *NC-CC dichotomy* most likely reflects a spatial separation of two genetically distinct reservoirs in the protoplanetary disk, which has far-reaching implications for the formation and early evolution of the Solar System (Bermingham et al., 2020; Kleine et al., 2020; Kruijer et al., 2020; Warren, 2011).

Furthermore, Mo isotopes can provide critical insights into Earth's accretion history and, by extension, into the origin of its habitability and the general dynamics of planet formation. Due to its moderately siderophile character, most of the Mo delivered to Earth was partitioned into its core, meaning that the Mo in the present-day bulk silicate Earth (BSE) derives almost exclusively from the late stages of accretion (*i.e.*, during or after the giant Moon-forming impact and the cessation of core formation). Hence, the Mo isotope signature of BSE holds valuable information on the integrated composition, and thus on the origin, of the material accreted to Earth during the last ~10–20 % of its growth history (Dauphas, 2017). As a result of >4 billion years of geological activity and convective stirring, the Earth's mantle is generally assumed to be well homogenized with respect to such nucleosynthetic anomalies. However, growing evidence for the existence of primordial mantle domains (*e.g.*, Bennett et al., 2007; Touboul et al., 2012), combined with the recent discovery of nucleosynthetic Ru isotope anomalies in some

* Corresponding author at: Department of Earth, Environmental and Planetary Sciences, Brown University, Providence, RI 02912, USA.
E-mail address: gerrit_budde@brown.edu (G. Budde).

https://doi.org/10.1016/j.chemer.2023.126007
Received 10 April 2023; Received in revised form 13 June 2023; Accepted 15 June 2023
Available online 16 June 2023
0009-2819/

Archaean rocks (Fischer-Gödde et al., 2020), suggests that some heterogeneities might have existed during Earth's early formative period and even been preserved until today. Such anomalous portions of the mantle might, for example, lack certain late-accreted components, potentially leading to small nucleosynthetic Mo isotope variations, which could have been recorded in some ancient or (modern) deep mantle-derived rocks. The discovery of such isotopic anomalies, relative to the BSE composition, would allow identifying specific building blocks of the Earth as well as better assessing the extent to which the nature of its accreted material changed over time.

However, both the precise determination of the mass-independent Mo isotope composition of BSE (*i.e.*, with respect to nucleosynthetic isotope variations) and the reliable identification of potential nucleosynthetic anomalies in terrestrial rocks require highly precise and accurate data. State-of-the-art techniques for multicollector inductively-coupled plasma mass spectrometry (MC-ICP-MS; Budde et al., 2016; Poole et al., 2017) and negative thermal ionization mass spectrometry (N-TIMS; Nagai and Yokoyama, 2016; Worsham et al., 2016; Yobregat et al., 2022) are capable of determining Mo isotope ratios with the required uncertainty of <10 ppm. At this level of precision, however, certain complications regarding the accuracy of the data can become significant; most notably, the effects of mass-dependent isotope fractionation. This is because, in order to isolate the genuine mass-independent anomalies from the measured data, it is essential to fully eliminate any natural and analytical mass fractionation. For this, the data are internally normalized to a given isotope ratio, where it is commonly assumed that all mass-dependent fractionation is accurately described by the 'exponential law': $r_{2/1} = R_{2/1} \times (m_2/m_1)^{\beta}$, where r and R are the measured and true, respectively, abundance ratio of isotopes 2 and 1, m is the isotopic mass, and β is the fractionation factor (Russell et al., 1978). While this empirical law has in general proven to be adequate for correcting isotope fractionation in the mass spectrometer, processes in the laboratory and especially in nature can follow different mass fractionation laws. In such cases, the conventional 'internal normalization' using the exponential law can create significant spurious mass-independent anomalies, as has been demonstrated for several elements (Mg, Davis et al., 2015; Ca, Ti, Zhang et al., 2014).

For Mo, however, this potential problem has so far received little attention, despite the fact that previous studies have revealed large mass-dependent isotope variations in terrestrial samples (total range of >1.3 ‰/amu), which are typically interpreted to reflect non-exponential (equilibrium or Rayleigh) fractionation processes (Kendall et al., 2017; Willbold and Elliott, 2017). To address this issue, we obtained new high-precision Mo isotope data for a diverse set of highly-fractionated terrestrial samples with the aim to constrain how pronounced and widespread such non-exponential fractionation is in nature and, ultimately, to assess its potential impact on internally normalized Mo isotope data. As such, this study highlights the need for a careful data examination in current and future studies that use nucleosynthetic Mo isotope anomalies in order to constrain Earth's accretion history (*e.g.*, Bermingham et al., 2022; Touboul et al., 2021).

2. Materials and methods

The samples investigated in this study include several kimberlites, continental and marine sediments, and the NIST 'SRM 129c' high-sulfur steel; sample types that have a high likelihood of being affected by significant mass-dependent Mo isotope fractionation (*e.g.*, Kendall et al., 2017). The kimberlites are from different occurrences in sub-Saharan Africa and have been analyzed for W isotopes in a previous study (Tappe et al., 2020). All continental sediments (mostly claystone and shale) derive from the Denver Basin (Colorado, USA), while the marine sediments (calcareous clays) are from the Frontale section at the Umbria-Marche Basin (Italy) and the Caravaca Basin (Spain). Additionally, aliquots of the geological reference material 'BHVO-2' and two Mo solution standards (see below) were processed (with and without sample matrix) through the entire analytical protocol (with Mo amounts of ~1 μg, which is the typical value for most samples), in order to assess the accuracy and precision of our procedures.

Sample preparation and digestion, the chemical separation of Mo, and the isotope measurements were conducted in the Institut für Planetologie at the University of Münster ('IfP') as well as in the Isotoparium at the California Institute of Technology ('CIT'), and followed our previously established protocols (Budde et al., 2019). In short, cleaned and powdered samples of ~0.2–1 g were digested in PFA vials on a hotplate using mixtures of concentrated HF–HNO_3(–$HClO_4$) and HCl–HNO_3. Mo was then separated from the sample matrix by anion exchange chromatography (using Bio-Rad *AG1-X8* resin), where Mo was eluted in dilute HNO_3. For the kimberlites, the extra clean-up step that is performed for selected samples was critical for eliminating their high Nb contents. Subsequently, all Mo cuts were further purified using Eichrom *TRU* extraction chromatography resin to remove any remaining matrix elements (*e.g.*, Fe/Mo was $<1 \times 10^{-3}$) and minimize isobaric interferences from Zr and Ru (Ru/Mo and Zr/Mo were $\ll 1 \times 10^{-4}$). The Mo yield for the entire procedure was typically ~70–80 %, and total procedural blanks were ~ 4 ng Mo and thus negligible. Mo concentrations were determined on small aliquots using a Thermo Scientific *XSeries 2* (IfP) or *iCAP RQ* (CIT) quadrupole ICP-MS.

The Mo isotope compositions were determined using Thermo Scientific Neptune *Plus* MC-ICP mass spectrometers, equipped with a Cetac Aridus II (IfP) or Aridus3 (CIT) desolvator and a combination of standard sampler and H skimmer (Ni) cones. The analyses were performed in low-resolution mode using analyte concentrations of ~100 ng/ml Mo and an integration time of 100 × 8.4 s per measurement, which consumed ~80 ng Mo. The mass-dependent data are reported as δ-unit (*i.e.*, parts per 1000) deviations relative to the bracketing solution standard, where $\delta^{98}Mo = [(^{98}Mo/^{95}Mo)_{sample}/(^{98}Mo/^{95}Mo)_{standard} - 1] \times 10^3$. We have not utilized a double-spike here because the respective laboratories were not equipped for such analyses at the time of our study; however, as we will discuss in Section 4, this is inconsequential for the conclusions of this study. The internally normalized data were obtained from the same measurements, by correcting mass fractionation using $^{98}Mo/^{96}Mo = 1.453173$ and the exponential law, as conventionally done in Mo isotope studies (*e.g.*, Bermingham et al., 2018; Budde et al., 2019; Poole et al., 2017; Yokoyama et al., 2019). These (mass-independent) data are reported as ε-unit (*i.e.*, parts per 10,000) deviations relative to the bracketing solution standard, where $\varepsilon^i Mo = [(^iMo/^{96}Mo)_{sample}/(^iMo/^{96}Mo)_{standard} - 1] \times 10^4$ (i = 92, 94, 95, 97, 100).

Of note, the two bracketing solution standards Alfa Aesar (prepared from Puratronic Mo powder, lot# C24P28; IfP) and NIST SRM 3134 (lot# 130418; CIT) used in the course of this study have virtually identical ε^iMo (mass-independent) compositions (Table 1), meaning that both subsets of ε^iMo data are directly comparable. However, our cross-calibration also reveals that they display very different degrees of mass-dependent fractionation; for consistency, all δ^{98}Mo values are thus reported relative to the commonly used SRM 3134.

3. Results

The Mo concentration and isotope data for the samples investigated in this study are summarized in Table 1. Their Mo concentrations vary typically between about 0.3 and 7 μg/g, while kimberlite 'K18' and sediment 'KT17' are characterized by exceptionally high values of 58 and 13 μg/g, respectively. The samples show substantial variations in the internally normalized isotope data (using the exponential law) that are mostly resolved from the solution standards. Their magnitude generally decreases in the order $\varepsilon^{92}Mo > \varepsilon^{94,100}Mo > \varepsilon^{95}Mo > \varepsilon^{97}Mo$, where the anomaly in ε^{97}Mo is often in the opposite direction to the other ε^iMo (Fig. 1). The ε^{92}Mo range from about −0.4 to +1.0, and the samples broadly follow a single correlation line in diagrams of ε^iMo *versus* ε^jMo (Fig. 2). Similarly, the samples show large and mostly resolved mass-dependent isotope variations with measured δ^{98}Mo

Table 1
Summary of Mo isotope data investigated in this study.

ID	Sample	Lab.	Mo (μg/g)	ε^{92}Mo	±	ε^{94}Mo	±	ε^{95}Mo	±	ε^{97}Mo	±	ε^{100}Mo	±	N	δ^{98}Mo (meas.)	δ^{98}Mo (corr.)	F (‰/amu)
Kimberlites																	
K11	LES17-02	IfP	0.84	−0.36	0.15	−0.10	0.12	0.05	0.06	0.08	0.04	−0.19	0.07	10	0.43	1.06	0.35
K14	ITA-1	IfP	4.43	−0.08	0.08	−0.05	0.04	0.04	0.04	0.02	0.05	0.02	0.06	9	−0.57	0.05	0.02
K18	NAM18-02	IfP	57.88	0.23	0.11	0.08	0.05	0.07	0.06	0.04	0.04	0.14	0.10	10	−1.49	−0.86	−0.29
K20	SAF18-57	IfP	7.39	0.16	0.10	0.10	0.04	0.11	0.04	0.08	0.05	0.03	0.03	10	−1.33	−0.70	−0.23
K22	LES17-02 (repl.)	IfP	0.79	−0.33	0.18	−0.11	0.13	0.05	0.09	0.10	0.08	−0.17	0.11	6	0.11	0.74	0.25
K23	LES17-01	IfP	0.30	−0.36	0.19	−0.04	0.19	0.05	0.09	0.11	0.13	−0.21	0.15	5	0.90	1.53	0.51
K24	LES17-03	IfP	0.20	0.36	0.16	0.10	0.24	0.14	0.14	0.02	0.21	0.12	0.08	4	−1.40	−0.77	−0.26
K25	ANG14-287	IfP	2.85	−0.19	0.09	−0.08	0.08	0.00	0.05	0.05	0.05	−0.11	0.09	8	−0.38	0.25	0.08
K26	SAF17-15	IfP	1.26	−0.02	0.24	0.01	0.17	0.09	0.12	0.09	0.08	−0.10	0.14	5	−0.39	0.24	0.08
K27	Igwisi Hills	IfP	0.38	0.12	0.21	0.09	0.09	0.11	0.02	0.10	0.03	−0.04	0.07	5	−0.76	−0.13	−0.04
K30	SAF18-58	IfP	1.23	−0.08	0.19	−0.02	0.13	0.07	0.10	0.06	0.06	−0.06	0.11	6	−0.43	0.20	0.07
Sediments																	
KT02	Frontale	CIT	1.35	0.66	0.10	0.22	0.07	0.12	0.08	0.02	0.07	0.27	0.11	6	−1.79	−1.16	−0.39
KT03	Caravaca	CIT	1.82	1.04	0.09	0.31	0.07	0.13	0.05	−0.05	0.02	0.42	0.05	8	−3.26	−2.63	−0.88
KT17	Denver Basin	CIT	13.13	−0.06	0.09	−0.04	0.03	0.02	0.04	0.02	0.04	−0.03	0.05	9	−0.55	0.08	0.03
KT18	Denver Basin	CIT	4.24	0.18	0.09	0.02	0.07	0.06	0.04	0.03	0.03	0.11	0.05	11	−1.19	−0.56	−0.19
KT19	Denver Basin	CIT	6.59	0.18	0.11	−0.01	0.07	0.04	0.06	0.02	0.04	0.10	0.06	9	−1.09	−0.46	−0.15
KT20	Denver Basin	CIT	4.35	0.14	0.15	0.01	0.06	0.07	0.05	0.02	0.08	0.07	0.04	5	−1.35	−0.72	−0.24
KT21	Denver Basin	CIT	6.20	0.19	0.07	0.04	0.06	0.05	0.03	0.02	0.03	0.10	0.07	11	−1.10	−0.47	−0.16
KT23	Denver Basin	CIT	1.26	0.12	0.11	0.00	0.06	0.07	0.06	0.06	0.02	0.17	0.07	7	−0.90	−0.27	−0.09
Others																	
N9C02,3,4	NIST SRM 129c	IfP[b]	7.42	−0.29	0.07	−0.08	0.04	0.00	0.03	0.03	0.03	−0.16	0.04	35	0.10	0.73	0.24
BHV27	BHVO-2	IfP	3.81	0.01	0.10	0.00	0.09	0.05	0.05	0.05	0.03	−0.03	0.07	9	−0.89	−0.26	−0.09
BHV36	BHVO-2	CIT	3.84	−0.02	0.12	−0.03	0.10	0.02	0.06	0.03	0.03	−0.01	0.04	9	−0.60	0.03	0.01
BHV39	BHVO-2	CIT	3.66	−0.03	0.10	−0.04	0.08	0.02	0.03	0.04	0.03	0.05	0.05	11	−0.61	0.02	0.01
K31	Proc. sol. std.[a]	IfP	–	0.05	0.14	0.05	0.07	0.08	0.04	0.04	0.05	0.00	0.09	8	−0.88	−0.26	−0.09
DI33	Proc. sol. std.	IfP[b]	–	0.00	0.15	−0.01	0.11	0.03	0.07	0.06	0.03	0.00	0.08	10	−0.62	0.01	0.00
CT45	Proc. sol. std.	CIT	–	−0.02	0.12	0.00	0.06	0.01	0.05	0.04	0.04	−0.02	0.06	11	−0.39	0.24	0.08
Δ(AA–3134)	Cross-calibrat.	CIT	–	−0.01	0.04	−0.01	0.03	0.00	0.02	0.00	0.02	0.04	0.02	66	−0.58	–	−0.19

The ε^{i}Mo were obtained by internal normalization to $^{98}Mo/^{96}Mo = 1.453173$ using the exponential law, and are reported relative to the Alfa Aesar ('AA'; IfP) or NIST SRM 3134 ('3134'; CIT), which have virtually identical ε^{i}Mo compositions. All δ^{98}Mo are reported relative to SRM 3134; 'corr.' values were corrected for an analytical mass fractionation effect (Section 4.1). Reported uncertainties for the ε^{i}Mo values represent the 95 % confidence interval of repeated measurements; for δ^{98}Mo, the external reproducibility is 0.20 ‰ for the measured (Section 3) and 0.28 ‰ for the corrected values (propagated uncertainties). N: number of analyses; $F = \delta^{98}Mo_{corr.}/(m^{98}Mo–m^{95}Mo)$.

[a] Kimberlite matrix (devoid of its natural Mo) doped with Mo from the Alfa Aesar solution standard before processing.

[b] Mass-independent data previously reported in Budde et al. (2018, 2019).

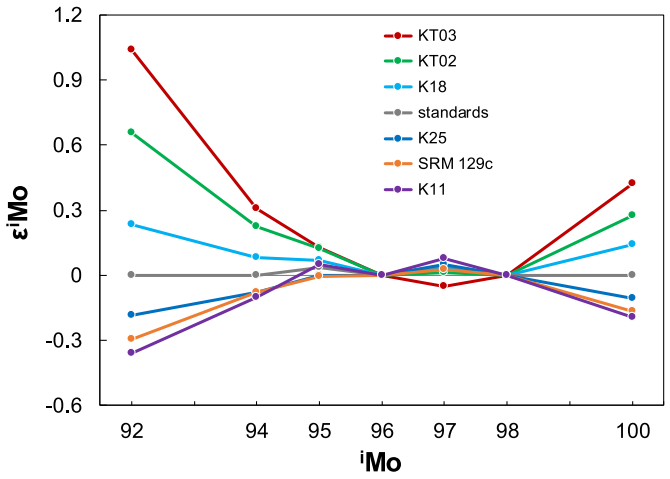

Fig. 1. Mo isotope patterns for selected samples showing the (apparent) mass-independent anomalies, after internal normalization using the exponential law and $^{98}Mo/^{96}Mo$. The investigated samples show both negative and positive $\varepsilon^{i}Mo$ anomalies, but always a characteristic *U*-shaped pattern. Error bars are omitted for clarity; 'standards' represents average of processed BHVO-2 and solution standards (see Section 3).

between about −3.3 ‰ (sediment 'KT03') and + 0.9 ‰ (kimberlite 'K23'), corresponding to a total range of ~1.4 ‰/amu.

Interestingly, the degree of mass-dependent isotope fractionation is strongly correlated with the apparent mass-independent anomalies, as demonstrated in Fig. 3. Using the measured $\delta^{98}Mo$, the samples define a regression line that does not pass through the origin but intercepts the *x*-axis ($\varepsilon^{92}Mo = 0$) at a $\delta^{98}Mo$ of −0.65 ± 0.08 ‰ (95 % CI, $n = 20$). Of note, the processed aliquots of the geological reference material BHVO-2 and the solution standards ('DI33', 'CT45', 'K31') show no $\varepsilon^{i}Mo$ anomalies, but an almost identical shift toward negative $\delta^{98}Mo$ with an average deviation of −0.63 ± 0.20 ‰ (95 % CI, $n = 6$) from their accepted/true value (−0.07 ‰ for BHVO-2, Willbold et al. (2016); ≡0 ‰ for the solution standards). After correction for this systematic offset (Section 4.1), the $\delta^{98}Mo$ range from about −0.9 to +1.5 ‰ for the kimberlites and about −2.6 to +0.1 ‰ for the sediments. These values generally fall within the range previously observed for igneous and sedimentary samples (Kendall et al., 2017; Willbold and Elliott, 2017); except for sediment 'KT03' ($\delta^{98}Mo = -2.6$ ‰) that, to our knowledge, represents the lightest Mo isotope compositions for natural samples measured to date.

4. Discussion

4.1. Origin of Mo isotope variations

Mass-dependent isotope fractionation can occur (*i*) during natural/geologic processes, (*ii*) during the chemical separation procedure, and (*iii*) in the mass spectrometer. The fact that the aliquots of BHVO-2 and the solution standards (with and without sample matrix) processed here show a consistent shift toward negative $\delta^{98}Mo$ with an average deviation of −0.63 ± 0.20 ‰ from their initial composition (see Section 3), demonstrates that significant mass fractionation was induced in the laboratory. Given the standard-sample bracketing applied here, any instrumental mass bias should be eliminated provided that solution standard and samples match closely in terms of concentration and purity (*e.g.*, Albarède et al., 2004), which was ensured in this study. Nonetheless, with this technique small matrix effects can still arise from unidentified impurities in the analyzed sample solutions. In such a case it is expected that the measured $\delta^{98}Mo$ would inversely correlate with the Mo amount, because of a decreasing impurity-to-Mo ratio with increasing amount of Mo (*e.g.*, Murphy et al., 2016); this is, however, not observed (Fig. S1). Since the Mo yield of our chromatographic separation was <90 %, another potential explanation is that the non-quantitative recovery of Mo was accompanied by mass-dependent fractionation, as has been documented for numerous elements including Mo (*e.g.*, Anbar et al., 2001; Siebert et al., 2001). For instance, Siebert et al. (2001) observed that the isotopic composition of the eluted Mo progressively changes from light to heavy, when anion exchange resin and dilute HNO_3 are used (comparable to our protocol). In such a case, an incomplete elution of Mo can result in negative $\delta^{98}Mo$ of the collected Mo cuts, which is generally consistent with the data in this study. The $\delta^{98}Mo$ obtained here, however, do not scale with the Mo yield of the chemical separation procedure (Fig. S1), as would be expected. Consequently, it remains unclear at what point exactly this analytical fractionation was induced. Of note, Pietruszka and Reznik (2008) observed in experiments that Mo added to solutions that were passed through anion exchange chromatography appeared isotopically light ($\delta^{98}Mo$ between −0.9 and −2.1 ‰). The authors attributed this to the presence of resin-derived organics in the analyzed solutions, changing the mass bias behavior relative to that of the unprocessed solution used for standard-sample bracketing. This so-called 'column matrix effect' is thus a combined chromatographic and instrumental effect and, given the overlap in the analytical protocols, a likely explanation for the offset observed here.

Importantly and independent of its exact origin, the mass-dependent analytical fractionation described above is roughly constant and seems to vary neither with the yield nor the amount of Mo processed. This is further supported by the analyzed kimberlite and sediment samples, which have much larger variations in $\delta^{98}Mo$ (incl. positive values), yield, and Mo amount (Fig. S1), but plot along a well-defined $\varepsilon^{92}Mo$–$\delta^{98}Mo$ regression line that is shifted by −0.65 ± 0.08 ‰ relative to the (unprocessed) SRM 3134 (Fig. 3). Of note, the samples display little scatter around this regression line, where the deviation is also independent of yield and Mo amount (Fig. S1). These observations indicate that these samples (*i*) have natural mass fractionation effects that are distinct from the analytical fractionation with respect to magnitude/direction as well as mechanism (see Section 4.2 for discussion), and (*ii*) experienced the same analytical fractionation as the processed standard materials. Based on the above findings, it can be assumed that the offset observed for the BHVO-2 and solutions standards is representative and that the analytical fractionation for the samples can thus be accurately corrected within the associated uncertainties, where $\delta^{98}Mo_{corr.} = \delta^{98}Mo_{meas.} + (0.63 \pm 0.20)$. For the following discussion, we will use the values thus obtained, because they provide the best representation of the natural mass-dependent effects in the kimberlite and sediment samples, which is supported by the fact that the regression line for the corrected $\delta^{98}Mo$ passes exactly through the current estimate for the BSE composition (Fig. 3).

As a result of the internal normalization applied here, any Mo isotope fractionation following the exponential law is cancelled out. Therefore, residual $\varepsilon^{i}Mo$ variations reflect mass-dependent fractionation that does not adhere to this law or, alternatively, mass-independent isotope anomalies. The latter can potentially have a nucleosynthetic (Dauphas et al., 2002) or a nuclear field shift (NFS; Fujii et al., 2006) origin. However, a close inspection of the Mo isotope patterns reveals that the investigated samples generally display a *U*-shaped pattern, which is very distinct from that for the NFS effect and the characteristic *W*-shaped pattern of nucleosynthetic anomalies (Fig. 4a). This is more clearly demonstrated in diagrams of $\varepsilon^{i}Mo$ *versus* $\varepsilon^{j}Mo$, showing the data relative to the distinct correlations lines defined by non-carbonaceous ('NC') and carbonaceous ('CC') materials, which reflect genuine nucleosynthetic isotope variations; *i.e.*, variable deficits in Mo nuclides produced in the slow neutron capture process ('*s*-process') (*e.g.*, Budde et al., 2019). In the $\varepsilon^{95}Mo$–$\varepsilon^{94}Mo$ diagram (Fig. 2a), which is typically used to illustrate this *NC-CC dichotomy*, the samples investigated here generally scatter around the current BSE estimate, supporting the previous conclusion that the BSE plots in between the NC- and CC-lines and that its Mo

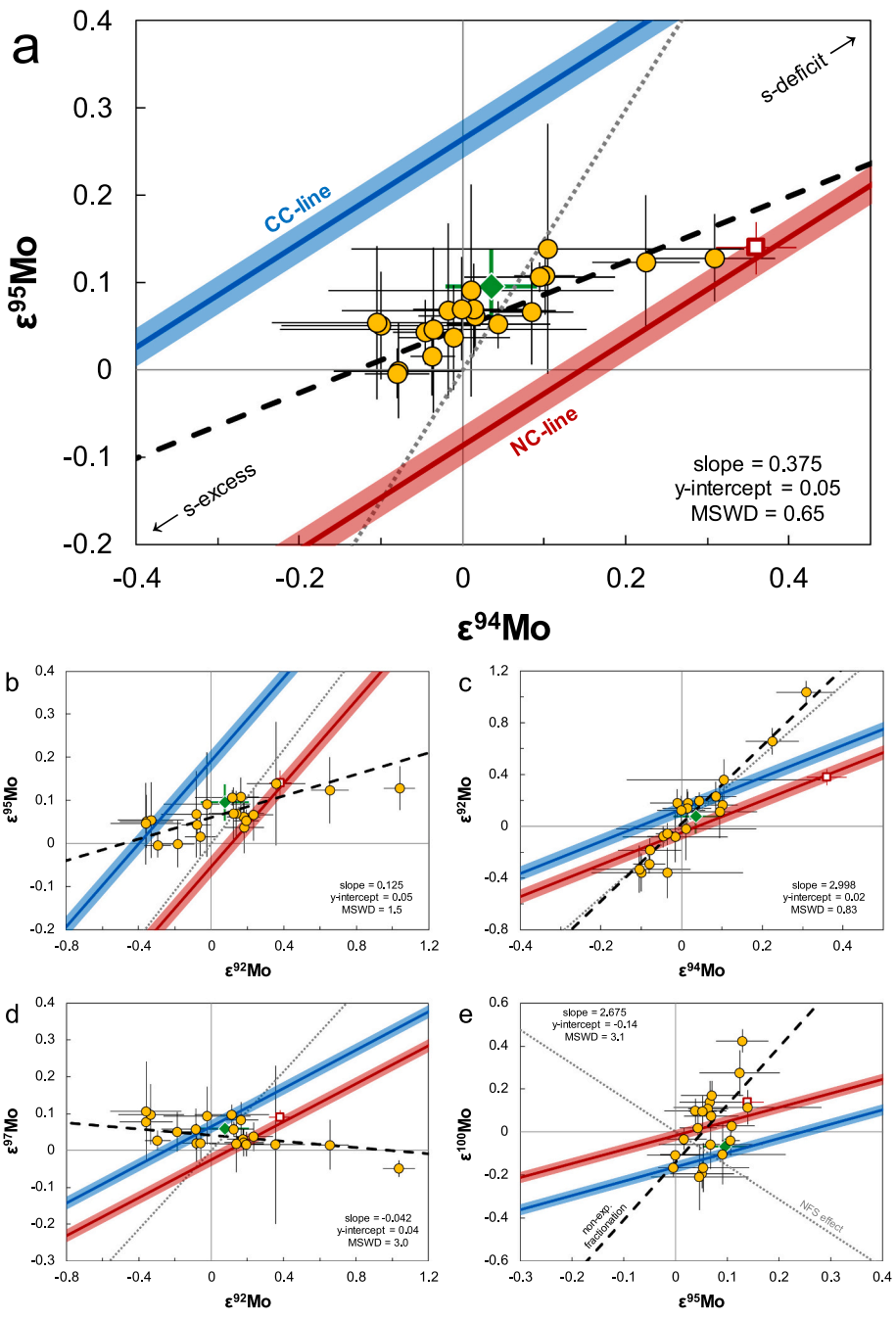

Fig. 2. Mo isotope diagrams showing the investigated samples (kimberlites, sediments, SRM 129c) in the context of the NC- and CC-lines (in red and blue, respectively). Dashed black lines represent predicted effects of non-exponential mass-dependent fractionation, calculated after Tang and Dauphas (2012); the respective intercepts are adjusted to best fit the sample data. Dotted gray lines represent theoretical effects of the nuclear field shift effect (NFS; see Fig. 4). Bulk silicate Earth estimate (green diamond) as well as NC- and CC-lines are based on data set from Budde et al. (2019); enstatite chondrites (red open square) are shown for reference (Render et al., 2017). (For interpretation of the references to colour in this figure legend, the reader is referred to the web version of this article.)

isotope composition, therefore, represents a mixture of inner (NC) and outer (CC) Solar System materials (Budde et al., 2019). However, many samples show clearly resolved deviations from the BSE value and some even overlap, within uncertainties, with the NC-line (near the position of enstatite chondrites). Taken at face value, this would be the first evidence for the preservation of nucleosynthetic Mo isotope anomalies in terrestrial rocks, which would in turn have far-reaching implications for Earth's accretion history. The other ε^{i}Mo–ε^{j}Mo diagrams (Fig. 2b–e), however, reveal fundamental inconsistencies with such an interpretation, as the samples plot at varying positions relative to the NC- and CC-lines and many even clearly beyond them. The latter is noteworthy because all known bulk Solar System materials (meteoritic and planetary) plot on or in between the NC/CC-lines, meaning that it is implausible that building blocks with such mass-independent Mo isotope compositions existed. It can, therefore, essentially be ruled out that the ε^{i}Mo variations obtained here have a mass-independent (nucleosynthetic or NFS) origin.

Consequently, these apparent anomalies most likely result from an inadequate correction of mass-dependent Mo isotope fractionation, which is supported by several lines of evidence. Various fractionation laws have been derived in the past (empirically and theoretically) in order to describe natural and analytical mass-dependent effects, where the most important are the exponential, equilibrium, Rayleigh, power, and linear fractionation laws. Except for the latter, these can be represented by the 'generalized power law' (GPL): $(r_{2/1}/R_{2/1}) = (r_{3/1}/R_{3/1})^{\theta}$ with $\theta = (m_2^n - m_1^n)/(m_3^n - m_1^n)$, where the differences between the individual laws are reflected by distinct values for n, which is a free parameter for the mass fractionation exponent (Maréchal et al., 1999). We note that, as a first-order approximation, the exponential law also describes kinetic isotope fractionation ($n \rightarrow 0$); the reader is referred to

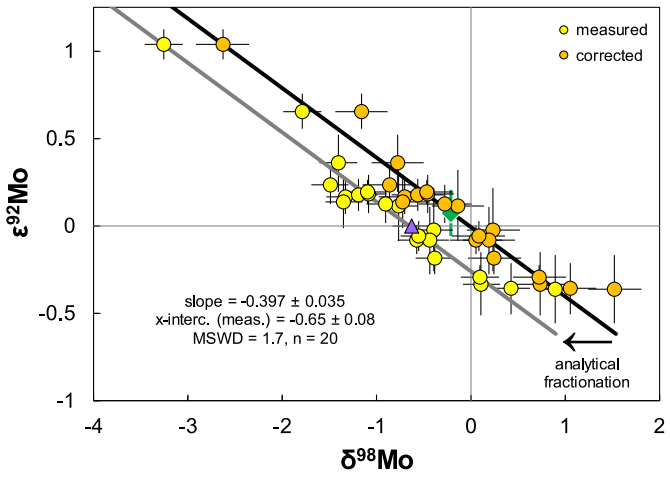

Fig. 3. Diagram of ε^{92}Mo *versus* δ^{98}Mo. The measured δ^{98}Mo of the samples show a systematic shift toward negative values (with δ^{98}Mo = −0.65 ‰ at ε^{92}Mo = 0), virtually identical to the average offset for processed BHVO-2 and solution standards (purple triangle). Due to its kinetic nature, this analytical mass-dependent fractionation shifts samples only horizontally (see Section 4). After its correction, the regression passes through the bulk silicate Earth estimate (green diamond; Budde et al., 2019; Greber et al., 2015). Regression calculated using the 'Model 1' of *IsoplotR* (v4.4); uncertainties represent 95 % CI. (For interpretation of the references to colour in this figure legend, the reader is referred to the web version of this article.)

Dauphas and Schauble (2016) for details. The differences between these laws are best illustrated when plotting their predicted effects as deviations from the conventionally used exponential law. As demonstrated in Fig. 5a, non-exponential Mo isotope fractionation results (when internally normalizing to ^{98}Mo/^{96}Mo using the exponential law) in characteristic *U*-shaped isotope patterns, where the anomaly in ε^{92}Mo is largest and that in ε^{97}Mo is smallest (and in the opposite direction), as observed for the samples investigated here. Of note, these systematics are also evident from the ε^{i}Mo–ε^{j}Mo diagrams (Fig. 2), where the samples generally follow the slopes for the predicted effects of non-exponential isotope fractionation.

Furthermore, as would be expected for an inadequate correction of mass fractionation, the ε^{i}Mo anomalies are strongly correlated with the degree of mass-dependent isotope fractionation (*F*). As illustrated in Fig. 5b, this also allows constraints to be placed on the underlying mechanism of mass fractionation, where the data obtained here are generally consistent with the predicted effects of the equilibrium and Rayleigh laws. This observation is in line with previous studies on mass-dependent Mo isotope fractionation in magmatic and sedimentary settings, which is often attributed to equilibrium or Rayleigh fractionation processes during sample formation or subsequent alteration/diagenesis (Kendall et al., 2017; and references therein). The heavy signature (δ^{98}Mo = +0.75 ‰) of the SRM 129c could have been inherited from its raw material or induced by non-exponential mass fractionation during its industrial production process. We note that, given their different formation histories, there is no reason to assume that the fractionation mechanism is the same for all samples here; however, they show little excess scatter (MSWD = 1.3) around a best-fit line with a slope corresponding to an *n*-value of −0.90, which is close to the fractionation exponent for canonical (high-temperature) equilibrium fractionation (*n* = −1; Fig. 5b). Regardless of the exact origin, the investigated samples clearly show large mass-dependent isotope variations that cannot be described by the exponential law, resulting in significant spurious mass-independent anomalies (after the conventional internal normalization) that have no significance for constraining Earth's accretion history.

4.2. Implications for Mo isotope analyses

The results obtained here by combining mass-dependent and mass-independent data have some important implications for the determination of Mo isotope compositions in general. First, the processed aliquots of the solution standards (with and without sample matrix) experienced significant mass-dependent fractionation of ~0.6 ‰ during the analytical procedure (consistent with the systematic δ^{98}Mo offset for the other samples; Fig. 3), but show no anomalies in the internally normalized (ε^{i}Mo) data. This strongly suggests that this analytical (chemistry-induced and/or instrumental) fractionation does indeed follow the exponential law and, therefore, represents (at least for the protocol applied here) most likely a kinetic rather than an equilibrium effect (*cf.* Anbar et al., 2001). This is noteworthy, as it means that the non-quantitative recovery of Mo during its chemical separation does not induce noticeable ε^{i}Mo anomalies when using the exponential law for the internal normalization. Similarly, the Alfa Aesar and NIST SRM 3134 solution standards used at the IfP and CIT, respectively, show a significant difference in mass-dependent fractionation (~0.2 ‰/amu), but have virtually identical ε^{i}Mo compositions (Table 1). This implies that the observed difference most likely results from kinetic isotope fractionation, and enables a direct comparison of the obtained mass-

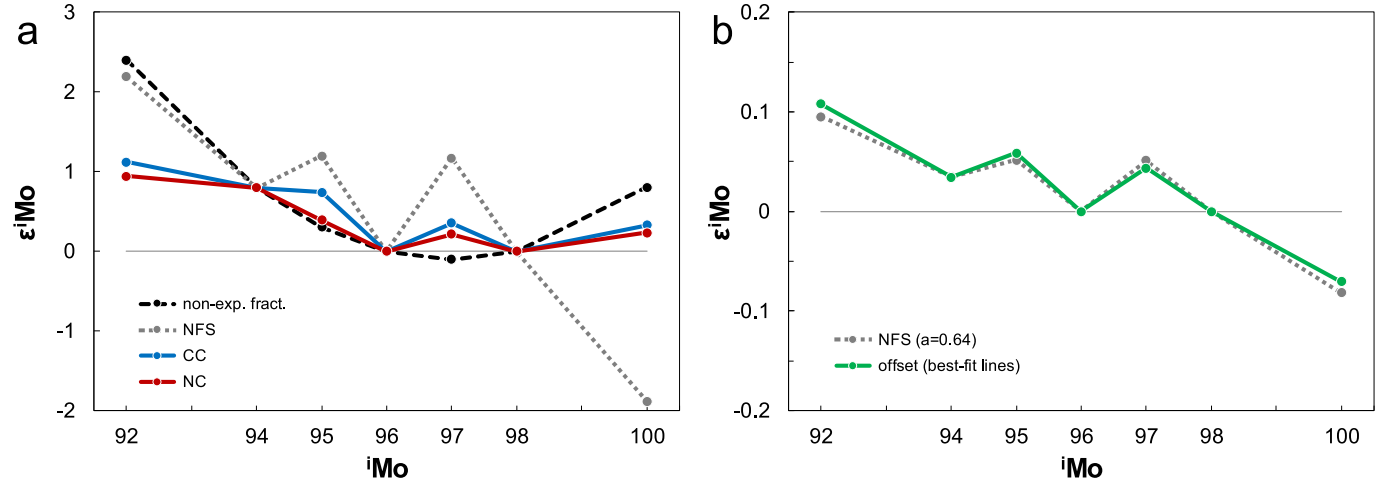

Fig. 4. Mass-dependent and mass-independent fractionation effects on internally normalized Mo isotope data, using the exponential law and ^{98}Mo/^{96}Mo. (a) Predicted effects of non-exponential mass fractionation, nucleosynthetic anomalies (for NC and CC materials), and the nuclear field shift effect (NFS); all patterns normalized to ε^{94}Mo = 0.8. (b) Offset of the best-fit lines in Fig. 2 (see Section 4.2 for discussion) compared to a small NFS effect. The latter was calculated after Fujii et al. (2006), using updated nuclear charge radii and isotope masses (Angeli and Marinova, 2013; Wang et al., 2021).

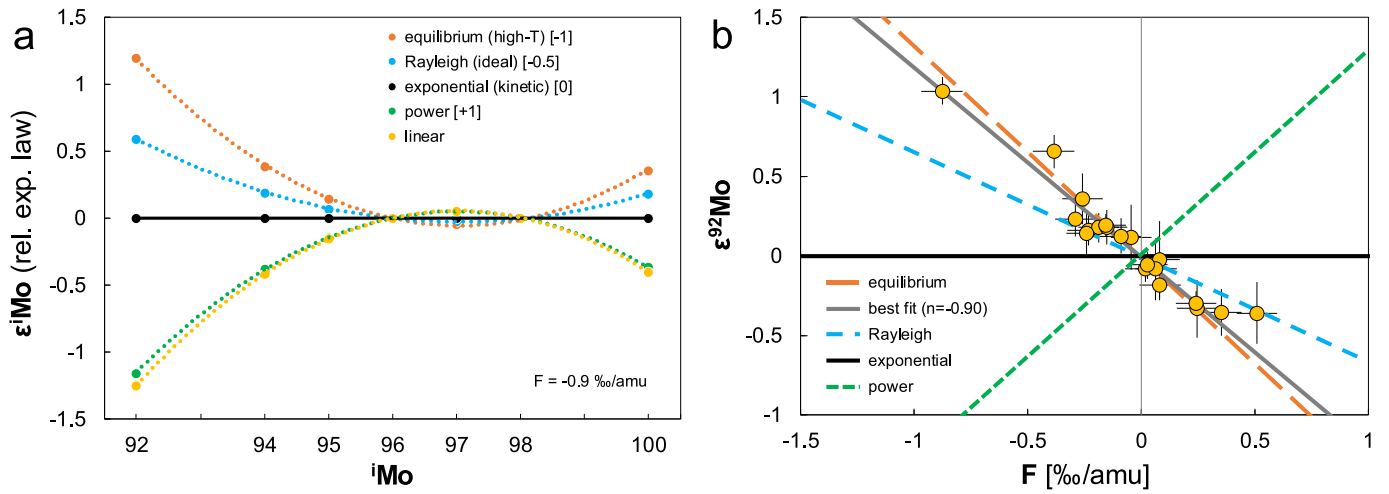

Fig. 5. Differences between various mass fractionation laws for Mo isotopes. (a) For a given degree of fractionation (*F*); reported as deviations from the exponential law (horizontal line). Values in square brackets refer to the *n*-value in the generalized power law (see Section 4.1). (b) Apparent mass-independent anomalies (here as ε^{92}Mo) as function of the degree of mass-dependent isotope fractionation (here in ‰/amu), which are inversely correlated. The best fit for the sample set (kimberlites, sediments, SRM 129c) is obtained for $n = -0.90$ in the generalized power law.

independent Mo isotope data sets. We note, however, that there is no *a priori* reason that this should always be the case, because those high-purity solution standards are typically made from Mo ores, which primarily represent molybdenites that can show substantial, often non-exponential, mass fractionation effects (Breillat et al., 2016).

Second, the ε^{i}Mo–ε^{j}Mo diagrams reveal that the best-fit lines for the samples analyzed here do not pass through the origin, which is the composition of the solution standards (Fig. 2). This small offset (that is also observed for the BSE estimate from Budde et al., 2019) cannot be explained by (non-exponential) mass fractionation, suggesting that it might represent a mass-independent effect instead. The overall ε^{i}Mo variations observed here are clearly inconsistent with a nuclear field shift effect, as both define very distinct correlation lines that are often nearly perpendicular (Fig. 2). However, the systematic offset of terrestrial rock samples from the solution standards (as evident from the non-zero intercepts of the best-fit lines) is best described by a slight deficit for ε^{100}Mo and slight excesses for the other ε^{i}Mo values (with $\varepsilon^{92}\text{Mo} > \varepsilon^{95,97}\text{Mo} > \varepsilon^{94}$Mo), which is characteristic of the NFS effect. Indeed, the intersection points of the best-fit lines and the theoretical NFS lines in Fig. 2 self-consistently define a Mo isotope composition that is consistent with a small NFS effect on the order of a few ppm (Fig. 4b). The available data is, unfortunately, not sufficient to evaluate whether this observation is significant and can indeed be attributed to a NFS effect, in which case it also remains unclear whether it reflects a roughly constant effect in the samples induced by the chemical separation procedure or whether it is a characteristic signature of the solution standards. The latter could potentially have been inherited from their raw material or induced during its (industrial) processing, which can cause exotic isotope effects in metal/steel samples (*e.g.*, SRM 129c) and solution standards made thereof (*e.g.*, Akram and Schönbächler, 2016; Budde et al., 2019; Steele et al., 2011; Zhang et al., 2012). We note that in both scenarios there is probably no noticeable impact on the conclusions from Budde et al. (2019) regarding the CC contribution to BSE's Mo (see below). This is because all terrestrial samples and most of those defining the NC- and CC-lines have been processed through the same analytical protocol and measured relative to the same solution standard. A potential small NFS effect, therefore, is expected to be rather invariable for this sample set, and would thus not significantly affect the BSE's position relative to the NC/CC-lines. Regardless, in line with previous findings (Fujii et al., 2006), the above demonstrates that assessing the extent of potential (natural or analytical) mass-independent isotope fractionation by the NFS effect will probably be important for obtaining Mo isotope data with high accuracy and for ensuring comparability between different protocols/data sets.

Finally and most importantly, our data is testament to widespread non-exponential mass fractionation and the first empirical evidence for its potential to create substantial spurious mass-independent Mo isotope anomalies. The fact that mass fractionation in all samples investigated here does not follow the exponential law strongly supports the previous theoretical, experimental, and empirical considerations (Kendall et al., 2017; Willbold and Elliott, 2017), concluding that equilibrium and Rayleigh (and not kinetic) processes are the dominant mechanisms of mass-dependent Mo isotope fractionation in natural systems. Depending on the degree of this non-exponential fractionation, using the exponential law for the internal normalization can then have fundamental effects on the evaluation of the measured Mo isotope data, if inappropriately interpreted as nucleosynthetic isotope anomalies. For example, in case of the largest degree of fractionation observed here (−0.9 ‰/amu), this can result in spurious anomalies of up to ~1.0 ε-unit (in ε^{92}Mo), which is on the same order of magnitude as genuine nucleosynthetic anomalies in bulk meteorites ($\varepsilon^{92}\text{Mo} \approx 0$–3; Budde et al., 2019). Further, in the ε^{95}Mo–ε^{94}Mo diagram (Fig. 2a), an inadequate correction of mass-dependent fractionation can lead to a significant apparent excess or deficit in *s*-process Mo nuclides and, in extreme cases, to samples overlapping with the NC- or CC-lines, respectively (as observed here for sediment 'KT03'). Of note, even a moderate degree of non-exponential fractionation of ~0.2 ‰/amu, can already result in deviations from the true $\varepsilon^{92,94,100}$Mo that exceed typical analytical uncertainties (Fig. 6a), which could, for instance, lead to the erroneous identification of isotopically anomalous domains in the silicate Earth. And even if the effects are smaller than the associated uncertainties (*i.e.*, on the order of several ppm), this can have significant consequences, as demonstrated in Fig. 6b. This figure illustrates the effect of non-exponential fractionation on the Δ^{95}Mo parameter, which represents a measure of the position relative to the NC/CC-lines in the ε^{95}Mo–ε^{94}Mo diagram (Fig. 2a) that can be used to calculate the fraction of CC-derived Mo in a given sample (*e.g.*, 46 ± 15 % for BSE; Budde et al., 2019). For instance, mass fractionation of only 0.2 ‰/amu would cause a shift in Δ^{95}Mo that corresponds to a difference of ~5 percentage points in the inferred CC-fraction, which can already have significant impact on constraining the nature and origin of Earth's late-state accretion materials.

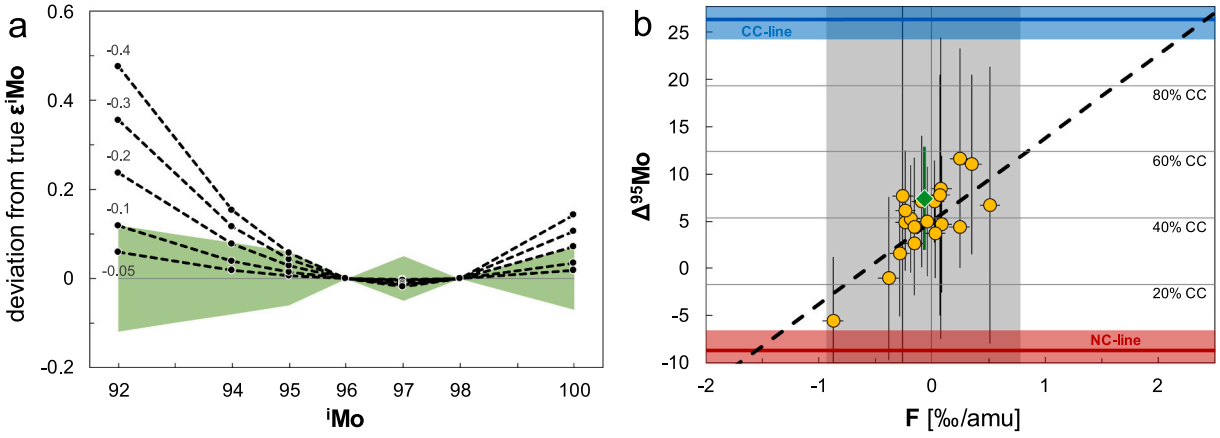

Fig. 6. Effects of non-exponential mass-dependent isotope fractionation on internally normalized Mo isotope data, based on the fractionation trend (n = −0.9) observed for the samples in Fig. 5b. (a) Effects in comparison to the analytical uncertainties (green band represents typical values for samples analyzed here); labels mark the degree of mass-dependent fractionation in ‰/amu. (b) Effects on Δ^{95}Mo [= (ε^{95}Mo − 0.596 × ε^{94}Mo) × 100]; intercept of dashed line is adjusted to best fit the sample data. Horizontal lines indicate inferred fraction of CC-derived Mo (see Budde et al., 2019); vertical gray bar represents the total range of mass-dependent fractionation observed in natural samples (this study; Kendall et al., 2017). See Figs. 2 and 3 for further details. (For interpretation of the references to colour in this figure legend, the reader is referred to the web version of this article.)

5. Conclusions

The high-precision Mo isotope data obtained in this study provide further evidence for widespread mass-dependent Mo isotope fractionation by equilibrium and Rayleigh processes in terrestrial samples, highlighting that it cannot generally be assumed that natural mass fractionation effects are adequately corrected for by the conventional internal normalization using the exponential law. As we demonstrate here, this can lead to substantial spurious mass-independent Mo isotope anomalies and, when misinterpreted as nucleosynthetic anomalies, to erroneous conclusions. This is particularly relevant for samples with complex geological histories including diagenetic or fluid-assisted processes (*e.g.*, marine sediments, molybdenites), but can also be significant for some igneous rocks. Additionally, while most bulk meteorites show only small (<0.3 ‰/amu) fractionation effects (Burkhardt et al., 2014), an inadequate mass fractionation correction can potentially be relevant for some extraterrestrial samples, in particular those with extensive condensation/evaporation or aqueous alteration effects. However, this problem can be addressed by obtaining high-precision mass-dependent (ideally using the double-spike technique) and mass-independent data in combination, which will allow to assess the magnitude and origin of mass fractionation in a given sample. Based on those results, residual effects on the internally normalized (ε^{i}Mo) values from an inappropriate mass fractionation correction can be ruled out or identified, and potentially mitigated by applying a more adequate fractionation law for the internal normalization. Combined, this will not only shed new light on the mechanisms of natural Mo isotope fractionation in general, but also be essential for applications that require a high level of accuracy, such as the precise determination of the mass-independent Mo isotope composition of bulk silicate Earth (with respect to the NC and CC reservoirs) and the reliable identification of potential nucleosynthetic anomalies in terrestrial rocks.

Supplementary data to this article can be found online at https://doi.org/10.1016/j.chemer.2023.126007.

Declaration of competing interest

There are no competing interests to declare.

Acknowledgments

We are grateful to S. Tappe (UiT) for providing the kimberlite samples, A. Montanari (OGC) for providing the Frontale sample, and the Denver Museum of Nature & Science for providing the Denver Basin samples (on loan to S. Bowring, MIT). This study was supported by the Deutsche Forschungsgemeinschaft (DFG, German Research Foundation) – Project-ID 263649064 – TRR 170 (to T.K.) and a Geochemistry Option Postdoctoral Fellowship by Caltech (to G.B.). F.T. is grateful for support from a Walter De Logi grant from Caltech for 2019–2021, the Caltech Center for Comparative Planetary Evolution, National Science Foundation (NSF) grants EAR-1824002 and MGG-2054892, a Packard Fellowship, a research award from the Heritage Medical Research Institute, and start-up funds provided by Caltech. We thank several reviewers for their constructive comments on different versions of this manuscript. This is TRR 170 publication no. 195.

References

Akram, W., Schönbächler, M., 2016. Zirconium isotope constraints on the composition of Theia and current Moon-forming theories. Earth Planet. Sci. Lett. 449, 302–310. https://doi.org/10.1016/j.epsl.2016.05.022.

Albarède, F., Telouk, P., Blichert-Toft, J., Boyet, M., Agranier, A., Nelson, B., 2004. Precise and accurate isotopic measurements using multiple-collector ICPMS. Geochim. Cosmochim. Acta 68, 2725–2744. https://doi.org/10.1016/j.gca.2003.11.024.

Anbar, A.D., Knab, K.A., Barling, J., 2001. Precise determination of mass-dependent variations in the isotopic composition of molybdenum using MC-ICPMS. Anal. Chem. 73, 1425–1431. https://doi.org/10.1021/ac000829w.

Angeli, I., Marinova, K.P., 2013. Table of experimental nuclear ground state charge radii: an update. At. Data Nucl. Data Tables 99, 69–95. https://doi.org/10.1016/j.adt.2011.12.006.

Bennett, V.C., Brandon, A.D., Nutman, A.P., 2007. Coupled ^{142}Nd-^{143}Nd isotopic evidence for Hadean mantle dynamics. Science 318, 1907–1910. https://doi.org/10.1126/science.1145928.

Bermingham, K.R., Worsham, E.A., Walker, R.J., 2018. New insights into Mo and Ru isotope variation in the nebula and terrestrial planet accretionary genetics. Earth Planet. Sci. Lett. 487, 221–229. https://doi.org/10.1016/j.epsl.2018.01.017.

Bermingham, K.R., Füri, E., Lodders, K., Marty, B., 2020. The NC-CC isotope dichotomy: implications for the chemical and isotopic evolution of the early solar system. Space Sci. Rev. 216, 133. https://doi.org/10.1007/s11214-020-00748-w.

Bermingham, K.R., Tornabene, H.A., Meyer, B.S., Patel, A., Mojzsis, S.J., Walker, R.J., 2022. Siderophile genetics of late-stage terrestrial accretion: new constraints on the composition of Earth's building blocks. In: Lunar Planet. Sci. Conf. #1468.

Breillat, N., Guerrot, C., Marcoux, E., Négrel, Ph., 2016. A new global database of δ^{98}Mo in molybdenites: a literature review and new data. J. Geochem. Explor. 161, 1–15. https://doi.org/10.1016/j.gexplo.2015.07.019.

Budde, G., Burkhardt, C., Brennecka, G.A., Fischer-Gödde, M., Kruijer, T.S., Kleine, T., 2016. Molybdenum isotopic evidence for the origin of chondrules and a distinct genetic heritage of carbonaceous and non-carbonaceous meteorites. Earth Planet. Sci. Lett. 454, 293–303. https://doi.org/10.1016/j.epsl.2016.09.020.

Budde, G., Kruijer, T.S., Kleine, T., 2018. Hf-W chronology of CR chondrites: implications for the timescales of chondrule formation and the distribution of ^{26}Al in the solar

nebula. Geochim. Cosmochim. Acta 222, 284–304. https://doi.org/10.1016/j.gca.2017.10.014.
Budde, G., Burkhardt, C., Kleine, T., 2019. Molybdenum isotopic evidence for the late accretion of outer Solar System material to Earth. Nat. Astron. 3, 736–741. https://doi.org/10.1038/s41550-019-0779-y.
Burkhardt, C., Kleine, T., Oberli, F., Pack, A., Bourdon, B., Wieler, R., 2011. Molybdenum isotope anomalies in meteorites: constraints on solar nebula evolution and origin of the Earth. Earth Planet. Sci. Lett. 312, 390–400. https://doi.org/10.1016/j.epsl.2011.10.010.
Burkhardt, C., Hin, R.C., Kleine, T., Bourdon, B., 2014. Evidence for Mo isotope fractionation in the solar nebula and during planetary differentiation. Earth Planet. Sci. Lett. 391, 201–211. https://doi.org/10.1016/j.epsl.2014.01.037.
Dauphas, N., 2017. The isotopic nature of the Earth's accreting material through time. Nature 541, 521–524. https://doi.org/10.1038/nature20830.
Dauphas, N., Schauble, E.A., 2016. Mass fractionation laws, mass-independent effects, and isotopic anomalies. Annu. Rev. Earth Planet. Sci. 44, 709–783. https://doi.org/10.1146/annurev-earth-060115-012157.
Dauphas, N., Marty, B., Reisberg, L., 2002. Molybdenum evidence for inherited planetary scale isotope heterogeneity of the protosolar nebula. Astrophys. J. 565, 640–644. https://doi.org/10.1086/324597.
Davis, A.M., Richter, F.M., Mendybaev, R.A., Janney, P.E., Wadhwa, M., McKeegan, K.D., 2015. Isotopic mass fractionation laws for magnesium and their effects on ^{26}Al–^{26}Mg systematics in solar system materials. Geochim. Cosmochim. Acta 158, 245–261. https://doi.org/10.1016/j.gca.2015.01.034.
Fischer-Gödde, M., Elfers, B.-M., Münker, C., Szilas, K., Maier, W.D., Messling, N., Morishita, T., Van Kranendonk, M., Smithies, H., 2020. Ruthenium isotope vestige of Earth's pre-late-veneer mantle preserved in Archaean rocks. Nature 579, 240–244. https://doi.org/10.1038/s41586-020-2069-3.
Fujii, T., Moynier, F., Telouk, P., Albarède, F., 2006. Mass-independent isotope fractionation of molybdenum and ruthenium and the origin of isotopic anomalies in Murchison. Astrophys. J. 647, 1506–1516. https://doi.org/10.1086/505459.
Greber, N.D., Puchtel, I.S., Nägler, T.F., Mezger, K., 2015. Komatiites constrain molybdenum isotope composition of the Earth's mantle. Earth Planet. Sci. Lett. 421, 129–138. https://doi.org/10.1016/j.epsl.2015.03.051.
Kendall, B., Dahl, T.W., Anbar, A.D., 2017. The stable isotope geochemistry of molybdenum. Rev. Mineral. Geochem. 82, 683–732. https://doi.org/10.2138/rmg.2017.82.16.
Kleine, T., Budde, G., Burkhardt, C., Kruijer, T.S., Worsham, E.A., Morbidelli, A., Nimmo, F., 2020. The non-carbonaceous–carbonaceous meteorite dichotomy. Space Sci. Rev. 216, 55. https://doi.org/10.1007/s11214-020-00675-w.
Kruijer, T.S., Kleine, T., Borg, L.E., 2020. The great isotopic dichotomy of the early Solar System. Nat. Astron. 4, 32–40. https://doi.org/10.1038/s41550-019-0959-9.
Maréchal, C.N., Télouk, P., Albarède, F., 1999. Precise analysis of copper and zinc isotopic compositions by plasma-source mass spectrometry. Chem. Geol. 156, 251–273. https://doi.org/10.1016/S0009-2541(98)00191-0.
Murphy, K., Rehkämper, M., Kreissig, K., Coles, B., van de Flierdt, T., 2016. Improvements in Cd stable isotope analysis achieved through use of liquid–liquid extraction to remove organic residues from Cd separates obtained by extraction chromatography. J. Anal. At. Spectrom. 31, 319–327. https://doi.org/10.1039/C5JA00115C.
Nagai, Y., Yokoyama, T., 2016. Molybdenum isotopic analysis by negative thermal ionization mass spectrometry (N-TIMS): effects on oxygen isotopic composition. J. Anal. At. Spectrom. 31, 948–960. https://doi.org/10.1039/C5JA00381D.
Pietruszka, A.J., Reznik, A.D., 2008. Identification of a matrix effect in the MC-ICP-MS due to sample purification using ion exchange resin: an isotopic case study of molybdenum. Int. J. Mass Spectrom. 270, 23–30. https://doi.org/10.1016/j.ijms.2007.11.001.
Poole, G.M., Rehkämper, M., Coles, B.J., Goldberg, T., Smith, C.L., 2017. Nucleosynthetic molybdenum isotope anomalies in iron meteorites – new evidence for thermal processing of solar nebula material. Earth Planet. Sci. Lett. 473, 215–226. https://doi.org/10.1016/j.epsl.2017.05.001.
Render, J., Fischer-Gödde, M., Burkhardt, C., Kleine, T., 2017. The cosmic molybdenum-neodymium isotope correlation and the building material of the Earth. Geochem. Perspect. Lett. 3, 170–178. https://doi.org/10.7185/geochemlet.1720.
Russell, W.A., Papanastassiou, D.A., Tombrello, T.A., 1978. Ca isotope fractionation on the Earth and other solar system materials. Geochim. Cosmochim. Acta 42, 1075–1090. https://doi.org/10.1016/0016-7037(78)90105-9.
Siebert, C., Nägler, T.F., Kramers, J.D., 2001. Determination of molybdenum isotope fractionation by double-spike multicollector inductively coupled plasma mass spectrometry. Geochem. Geophys. Geosyst. 2, 2000GC000124 https://doi.org/10.1029/2000GC000124.
Steele, R.C.J., Elliott, T., Coath, C.D., Regelous, M., 2011. Confirmation of mass-independent Ni isotopic variability in iron meteorites. Geochim. Cosmochim. Acta 75, 7906–7925. https://doi.org/10.1016/j.gca.2011.08.030.
Tang, H., Dauphas, N., 2012. Abundance, distribution, and origin of ^{60}Fe in the solar protoplanetary disk. Earth Planet. Sci. Lett. 359–360, 248–263. https://doi.org/10.1016/j.epsl.2012.10.011.
Tappe, S., Budde, G., Stracke, A., Wilson, A., Kleine, T., 2020. The tungsten-182 record of kimberlites above the African superplume: exploring links to the core-mantle boundary. Earth Planet. Sci. Lett. 547, 116473 https://doi.org/10.1016/j.epsl.2020.116473.
Touboul, M., Puchtel, I.S., Walker, R.J., 2012. ^{182}W evidence for long-term preservation of early mantle differentiation products. Science 335, 1065–1069. https://doi.org/10.1126/science.1216351.
Touboul, M., Fitoussi, C., O'Neil, J., 2021. Exotic Mo isotope composition in the Nuvvuagittuq greenstone belt. In: Goldschmidt Conference. https://doi.org/10.7185/gold2021.7475.
Wang, M., Huang, W.J., Kondev, F.G., Audi, G., Naimi, S., 2021. The AME2020 atomic mass evaluation (II). Tables, graphs and references. Chin. Phys. C 45, 030003 https://doi.org/10.1088/1674-1137/abddaf.
Warren, P.H., 2011. Stable-isotopic anomalies and the accretionary assemblage of the Earth and Mars: a subordinate role for carbonaceous chondrites. Earth Planet. Sci. Lett. 311, 93–100. https://doi.org/10.1016/j.epsl.2011.08.047.
Willbold, M., Elliott, T., 2017. Molybdenum isotope variations in magmatic rocks. Chem. Geol. 449, 253–268. https://doi.org/10.1016/j.chemgeo.2016.12.011.
Willbold, M., Hibbert, K., Lai, Y.-L., Freymuth, H., Hin, R.C., Coath, C., Vils, F., Elliott, T., 2016. High-precision mass-dependent molybdenum isotope variations in magmatic rocks determined by double-spike MC-ICP-MS. Geostand. Geoanal. Res. 40, 389–403. https://doi.org/10.1111/j.1751-908X.2015.00388.x.
Worsham, E.A., Walker, R.J., Bermingham, K.R., 2016. High-precision molybdenum isotope analysis by negative thermalionization mass spectrometry. Int. J. Mass Spectrom. 407, 51–61. https://doi.org/10.1016/j.ijms.2016.06.005.
Yobregat, E., Fitoussi, C., Pili, E., Touboul, M., 2022. High-precision measurements of Mo isotopes by N-TIMS. Int. J. Mass Spectrom. 476, 116846 https://doi.org/10.1016/j.ijms.2022.116846.
Yokoyama, T., Nagai, Y., Fukai, R., Hirata, T., 2019. Origin and evolution of distinct molybdenum isotopic variabilities within carbonaceous and noncarbonaceous reservoirs. Astrophys. J. 883, 62. https://doi.org/10.3847/1538-4357/ab39e7.
Zhang, J., Dauphas, N., Davis, A.M., Leya, I., Fedkin, A., 2012. The proto-Earth as a significant source of lunar material. Nat. Geosci. 5, 251–255. https://doi.org/10.1038/NGEO1429.
Zhang, J., Huang, S., Davis, A.D., Dauphas, N., Hashimoto, A., Jacobsen, S.B., 2014. Calcium and titanium isotopic fractionations during evaporation. Geochim. Cosmochim. Acta 140, 365–380. https://doi.org/10.1016/j.gca.2014.05.022.